arXiv:1704.06186v1 [physics.ao-ph] 20 Apr 2017

On the significance of coherent Lagrangian eddies detected from satellite altimetry

M. J. Olascoaga[1,2], F. J. Beron-Vera[3], Y. Wang[4], J. Triñanes[5], and P. Pérez-Brunius[6]

[1]Department of Ocean Sciences, RSMAS, University of Miami, Miami, Florida, USA.

[2]Corresponding author. ***email:jolascoaga@rsmas.miami.edu***

[3]Department of Atmospheric Sciences, RSMAS, University of Miami, Miami, Florida, USA.

[4]Department of Atmospheric and Ocean Sciences, UCLA, Los Angeles, California, USA.

[5]Atlantic Oceanic and Atmospheric Laboratory, NOAA, Miami, Florida, USA; CIMAS, University of Miami, Miami, Florida, USA; and ITT, University of Santiago de Compostela, Santiago, Spain.

[6]CICESE, Ensenada, Baja California, México.

April 21, 2017

ABSTRACT

Ocean flows are routinely inferred from low-resolution satellite altimetry measurements of sea surface height (SSH) assuming a geostrophic balance. Recent nonlinear dynamical systems techniques have revealed that altimetry-inferred flows can support mesoscale eddies with material boundaries that do not filament for many months, thereby representing effective mechanisms for coherent transport. However, the significance of such coherent Lagrangian eddies is not free from uncertainty due to the impossibility of altimetry to resolve ageostrophic submesoscale motions, which have the potential of quickly eroding their boundaries. Using an unprecedented combination of satellite ocean color and surface drifter trajectory data, we provide observational evidence of an altimetry-inferred coherent Lagrangian Loop Current ring. We show that a velocity field derived using subsampled SSH from a submesoscale permitting ocean general circulation model simulation of the Gulf of Mexico supports a similar mesoscale coherent Lagrangian eddy, and further that the total surface velocity field produced by the model supports a well-organized swirling Lagrangian structure despite the enhanced submesoscale activity present in the simulation. Our results provide support to the idea that coherent Lagrangian eddies are not artifacts of the altimetry-derived flow but rather constitute real components of the ocean circulation.

List of Figures

1 In grey, contour levels of the altimetric sea surface height (SSH) field in the Gulf of Mexico (GoM) on selected days. Overlaid in blue are snapshots of the passive evolution, according to the altimetry-derived flow, of tracers initially on 29 May 2013 along the outermost of the closed SHH streamlines filling a mesoscale region of nearly 100-km radius in the center of the GoM, which has been identified as a Loop Current ring (LCR) and named *Kraken*. These closed instantaneous SSH streamlines are the Eulerian footprints of a coherent Lagrangian LCR, which nearly steadily translates westward across the GoM. The solid red curve is the boundary for the longest-lived and largest coherent Lagrangian LCR core. The dashed red curve is a material loop that provides repeated, short-term shielding to this core. 9

2 Satellite-derived chlorophyll concentration images on selected days with the altimetry-inferred long- (solid) and short-term (dashed) coherent Lagrangian boundaries of LCR *Kraken* overlaid. The top-right panel shows, as a function of time since 29 May 2013, area enclosed by the long- (solid red) and short-term (dashed red) Lagrangian boundaries, the outermost instantaneous closed SSH contour level (blue), and the area spanned by the chlorophyll deficient patch (green). 12

3 Snapshots of the evolution of the altimetry-inferred coherent Lagrangian long- (solid red) and short-term (dashed red) boundaries of LCR *Kraken* along with that of satellite-tracked surface drifters initially as close as 50 km from the long-term boundary (blue). The drifter positions on each day shown are indicated by blue dots. The tails attached to the dots are week-long past trajectory segments. One point on the long-term boundary is highlighted by a black dot surrounded by a circle, for reference. The top-right panel shows as a function of drifter lifespan, initial (black square) and mean (red triangle) shortest signed distance to the long-term boundary for all drifters initially lying within. 14

4 Snapshots of the evolution of the boundary of coherent Larangian LCR *Kraken* as extracted from altimetric SSH (red) and subsampled SSH from a submesoscale permitting Navy Coastal Model (NCOM) simulation of the GoM (blue), and a tracer patch passively advected by the surface model velocity (light blue). The top-right panel shows the mean distance to the corresponding centroid from points on the altimetry-derived boundary (red), the model SSH-derived boundary (blue), and the boundary of the tracer patch passively advected by the surface model velocity (light blue), each normalized by the value taken initially on 29 May 2013. The bottom-left panel is snapshot of the surface vorticity (normalized by the mean Coriolis parameter) field on 29 May 2013. 17

1. Introduction

Recent developments in the area of nonlinear dynamical systems have led to the possibility of detecting from a finite-time-aperiodic flow realization vortices or eddies with material (or Lagrangian, i.e., composed at all times of the same fluid particles) boundaries that experience no filamentation over the detection interval, irrespective of the ob-

server (Haller and Beron-Vera, 2012; Beron-Vera *et al.*, 2013; Haller and Beron-Vera, 2013; 2014; Haller, 2016; Haller *et al.*, 2016). Such coherent Lagrangian eddies have been extracted from flows derived geostrophically from satellite altimetric measurements of sea surface height (SSH) in a number of occasions (Beron-Vera *et al.*, 2015; Romero *et al.*, 2016; Wang *et al.*, 2015; 2016). While satellite altimetry is widely used to monitor global ocean variability (Beron-Vera *et al.*, 2008; 2010; Fu *et al.*, 2010), the significance of altimetry-inferred coherent Lagrangian eddies is surrounded by a certain degree of skepticism. The origin of this skepticism resides in the impossibility of altimetry to resolve submesoscale processes, which are increasingly believed to be important in the upper ocean (McWilliams, 2008; Klein, 2009; Poje *et al.*, 2014). Submesoscale processes should rapidly erode the boundary of any mesoscale coherent Lagrangian eddy detected from altimetry (Haza *et al.*, 2016).

The goal of this paper is to provide support to the significance of altimetry-derived mesoscale coherent Lagrangian eddies using an unprecedented combination of observations from independent sources and the output from a submesoscale permitting ocean general circulation model simulation. Specifically, we first detect from altimetry an exceptionally persistent coherent Lagrangian Loop Current ring (LCR) in the Gulf of Mexico (GoM). Then we show that associated with the ring is a satellite-derived chlorophyll deficient patch, confirming the material nature of the ring. Using satellite-tracked surface drifter trajectories we provide evidence that the boundary of the ring is largely convex (wiggle free), showing no significant signs of the presence of submesoscale eddies rolling up around its boundary. Finally, we show that the velocity field derived by subsampling the model's SSH supports a coherent Lagrangian ring with similar characteristics, and further that the total model surface velocity supports a well-organized swirling Lagrangian structure in its vicinity despite the rather intense simulated submesoscale activity.

2. Methods

a. Coherent Lagrangian eddies

Haller and Beron-Vera (Haller and Beron-Vera, 2013; 2014) seek fluid regions enclosed by exceptional material loops that defy the exponential stretching that a typical loop will experience in turbulent flow. As demonstrated by these authors, such loops, which constitute a type (elliptic) of coherent Lagrangian structure (Haller, 2015), have small annular neighborhoods exhibiting no leading-order variation in averaged material stretching.

Solving the above variational problem reveals that the loops in question are uniformly stretching: any of their subsets are stretched by the same factor λ under advection by the flow from time t_0 to time t. The time t_0 positions of λ-stretching material loops turn out to be limit cycles of one of the following two equations for parametric curves $s \mapsto x_0(s)$:

$$\frac{\mathrm{d}x_0}{\mathrm{d}s} = \sqrt{\frac{\lambda_2(x_0) - \lambda^2}{\lambda_2(x_0) - \lambda_1(x_0)}}\,\xi_1(x_0) \pm \sqrt{\frac{\lambda^2 - \lambda_1(x_0)}{\lambda_2(x_0) - \lambda_1(x_0)}}\,\xi_2(x_0), \tag{1}$$

where $\lambda_1(x_0) < \lambda^2 < \lambda_2(x_0)$. Here $\{\lambda_i(x_0)\}$ and $\{\xi_i(x_0)\}$, satisfying

$$0 < \lambda_1(x_0) \equiv \frac{1}{\lambda_2(x_0)} < 1, \quad \xi_i(x_0) \cdot \xi_j(x_0) = \delta_{ij} \quad i, j = 1, 2, \tag{2}$$

are eigenvalues and (normalized) eigenvectors, respectively, of the Cauchy–Green tensor,

$$C^t_{t_0}(x_0) := \mathrm{D}F^t_{t_0}(x_0)^\top \mathrm{D}F^t_{t_0}(x_0), \tag{3}$$

an objective (i.e., observer-independent) descriptor of material deformation, where $F^t_{t_0} : x_0 \mapsto x(t; x_0, t_0)$ is the flow map that takes time t_0 positions to time t positions of fluid particles, which obey

$$\frac{\mathrm{d}x}{\mathrm{d}t} = v(x, t), \tag{4}$$

where $v(x,t)$ is a divergenceless two-dimensional velocity field.

Limit cycles of (1) either grow or shrink under changes in λ, forming smooth annular regions of nonintersecting loops. The outermost member of such a band of material loops is observed physically as the boundary of a *coherent Lagrangian eddy*. Limit cycles of (1) tend to exist only for $\lambda \approx 1$. Material loops characterized by $\lambda = 1$ resist the universally observed material stretching in turbulence: they reassume their initial arclength at time t. This conservation of arclength, along with enclosed area preservation (which holds by assumption), produces extraordinary coherence (Beron-Vera *et al.*, 2013). Finally, limit cycles of (1) are (null) geodesics of the generalized Green–Lagrange tensor $C^t_{t_0}(x_0) - \lambda^2\,\mathrm{Id}$, which must necessarily contain degenerate points of $C^t_{t_0}(x_0)$ where its eigenvector field is isotropic. For this reason the above procedure is known as *geodesic eddy detection*.

The specific form of the velocity field considered here is given by

$$v(x,t) = \frac{g}{f}\nabla^{\perp}\eta(x,t), \tag{5}$$

where g is the acceleration of gravity, f stands for Coriolis parameter, and $\eta(x,t)$ is the SSH.

The numerical implementation of geodesic eddy detection is documented at length (Haller and Beron-Vera, 2012; 2013; Hadjighasem *et al.*, 2013; Haller and Beron-Vera, 2014; Karrasch *et al.*, 2014; Beron-Vera *et al.*, 2015; Haller, 2015; Wang *et al.*, 2015; Hadjighasem and Haller, 2016; Wang *et al.*, 2016). A software tool is also available (Onu *et al.*, 2015). Here we have set the grid width of the computational domain to 0.1 km. All integrations were carried out using a step-adapting fourth/fifth-order Runge–Kutta method with interpolations done with a cubic method.

b. Data

The SSH is taken as the sum of a (steady) mean dynamic topography and the (transient) altimetric SSH anomaly. The mean dynamic topography is constructed from satel-

lite altimetry data, in-situ measurements, and a geoid model (Rio and Hernandez, 2004). The SSH anomaly is provided weekly on a 0.25°-resolution longitude–latitude grid. This is referenced to a 20-year (1993–2012) mean, obtained from the combined processing of data collected by altimeters on the constellation of available satellites (Le Traon *et al.*, 1998).

The ocean color data consist of chlorophyll concentration fields obtained from the NASA Biology Processing Group website (http://oceancolor. gsfc.nasa.gov). Sun glint and clouds represent a major source of data gaps in the Gulf of Mexico, especially during the summer months. To minimize their effects and improve coverage, we have chosen to use multiday Level-3 mapped products. These are 8-day composite chlorophyll fields at 4-km horizontal resolution from the MODIS (Moderate Resolution Imaging Spectroradiometer) sensor, on-board NASAs EOS *Terra* and *Aqua* satellites, and the VIIRS (Visible Infrared Imaging Radiometer Suite) sensor, aboard the *Suomi-NPP* satellite.

The surface drifters are Far Horizon Drifters (FHD), manufactured by Horizon Marine, Inc. (Sharma *et al.*, 2010; Anderson and Sharma, 2008). They consist of a cylindrical buoy attached to a 45-m tether line, attached itself to a 1.2-m "para-drogue." These instruments are deployed by air, so the drogue serves both as parachute to protect the buoy when air deployed, as well as to reduce wind slippage of the buoy as it drifts in the water. Positions are recorded hourly using GPS and transmit the data via the *Argos* system. The quality control of the data consisted of interpolating positions between data gaps shorter than 6 hours, removing locations over land, and data points with speeds exceeding 3 m s^{-1}. Correlations of the drifter velocities with winds (Pérez-Brunius *et al.*, 2013) are of the same order as those obtained with the SVP drifters (Poulain *et al.*, 2009), which are drogued with a holey sock at about 15 m. This suggests that wind-slippage on the FHD drifter is minimal and the water-following characteristics of FHD drifters are in general similar the drifters used by the NOAA Global NOAA Global Drifter Program (Lumpkin and Pazos, 2007).

c. Model

The NCOM simulation employs assimilation and nowcast analyses from NCODA (Navy Coupled Ocean Data Assimilation) (Cummings, 2005). Forecasts are generated by systems linking NCODA with regional implementations (Rowley and Mask, 2014) of NCOM (Barron *et al.*, 2006). The model has 1-km horizontal resolution and was initiated on 15 May 2012 from the then operational global ocean model Global Ocean Forecast System (GOFS) 2.6 (Barron *et al.*, 2007). Daily boundary conditions are received from the current operational GOFS using the HYbrid Coordinate Ocean Model (HYCOM) (Metzger *et al.*, 2009). The vertical grid is comprised of 49 total levels; 34 terrain-following σ-levels above 550 m and 15 lower z-levels. The σ-coordinate structure has higher resolution near the surface with the surface layer having 0.5-m thickness. The simulation uses atmospheric forcing at the sea surface from COAMPS (Coupled Ocean/Atmosphere Mesoscale Prediction System) (NRL, 1997) to generate forecasts of ocean state out to 72 h in 3-hour increments. The observational data assimilated in these studies is provided by NAVOCEANO (Naval Oceanographic Office) and introduced into NCODA via its ocean data quality control process. Observations are three-dimensional variational (3D-Var) assimilated (Smith *et al.*, 2011) in a 24-hour update cycle with the first guess from the prior day NCOM forecast. The reliability of the model surface fields is supported on ability of the surface velocity to reproduce relative dispersion statistics (Beron-Vera and LaCasce, 2016) observed during the Grand LAgrangian Experiment (GLAD) (Olascoaga *et al.*, 2013), and the model SSH and surface velocity to capture observed Lagrangian coherence as we show here.

3. Results

The focus of our analysis is a region filled with closed streamlines of the altimetric SSH field in the GoM, which can be tracked for nearly one year since April 2013. The region was classified as an LCR by the Horizon Marine Inc.'s EddyWatch® program (http://

www.horizonmarine.com) using Leben's (Leben, 2005) methodology, which searches for Eulerian footprints of LCRs on the SSH field, and further named *Kraken*.

Figure 1 shows in grey several contour levels of the SSH field on three selected days, progressing from top to bottom. Highlighted in blue on the top is the outermost closed SSH contour in the region identified as LCR *Kraken* on the indicated day. Two images of this curve under the flow map associated with the altimetry-derived advection field are shown on the middle and bottom. More specifically, these are the result of integrating the passive tracer particle equation (4), with the velocity given by (5), from tracer positions initially on 29 May 2013 along the curve. Several additional frames, including instantaneous SSH isolines as well as advected images of the tracer curve along several months, are shown in Supplementary Movie S1.

Note the filamentation experienced by the passively advected tracer curve. Note also that, while intense, the filamentation is mainly outward. The outward-filamented curve portion reveals a number of swirling flow regions of varied sizes in the mesoscale range. Most of these are not seen to preserve their entity over time. The inward-filamented curve piece, by contrast, reveals a enduring compact region, of a mean radius of nearly 100 km, contained inside the region where the SSH streamlines are instantaneously closed and has been been identified as LCR *Kraken*. Two key observations about the behavior of the tracer near this region are in order. First, the tracer does not invade the region along the course of many months. Rather, it wraps around the region in an anticyclonic fashion. Second, the wrapping tracer tends to occupy a thick belt (with a width of 10 to 20 km) around the region in question. These two observations suggest on one hand that LCR *Kraken* has an impermeable material core, surrounded by a resilient material loop which acts as a long-term barrier for the transport of tracer into and out from the material core. On the other hand, outside this long-term closed transport barrier, shorter-term material barriers must be emerging repeatedly, shaping and confining the tracer wrapping around the long-term coherent Lagrangian ring core.

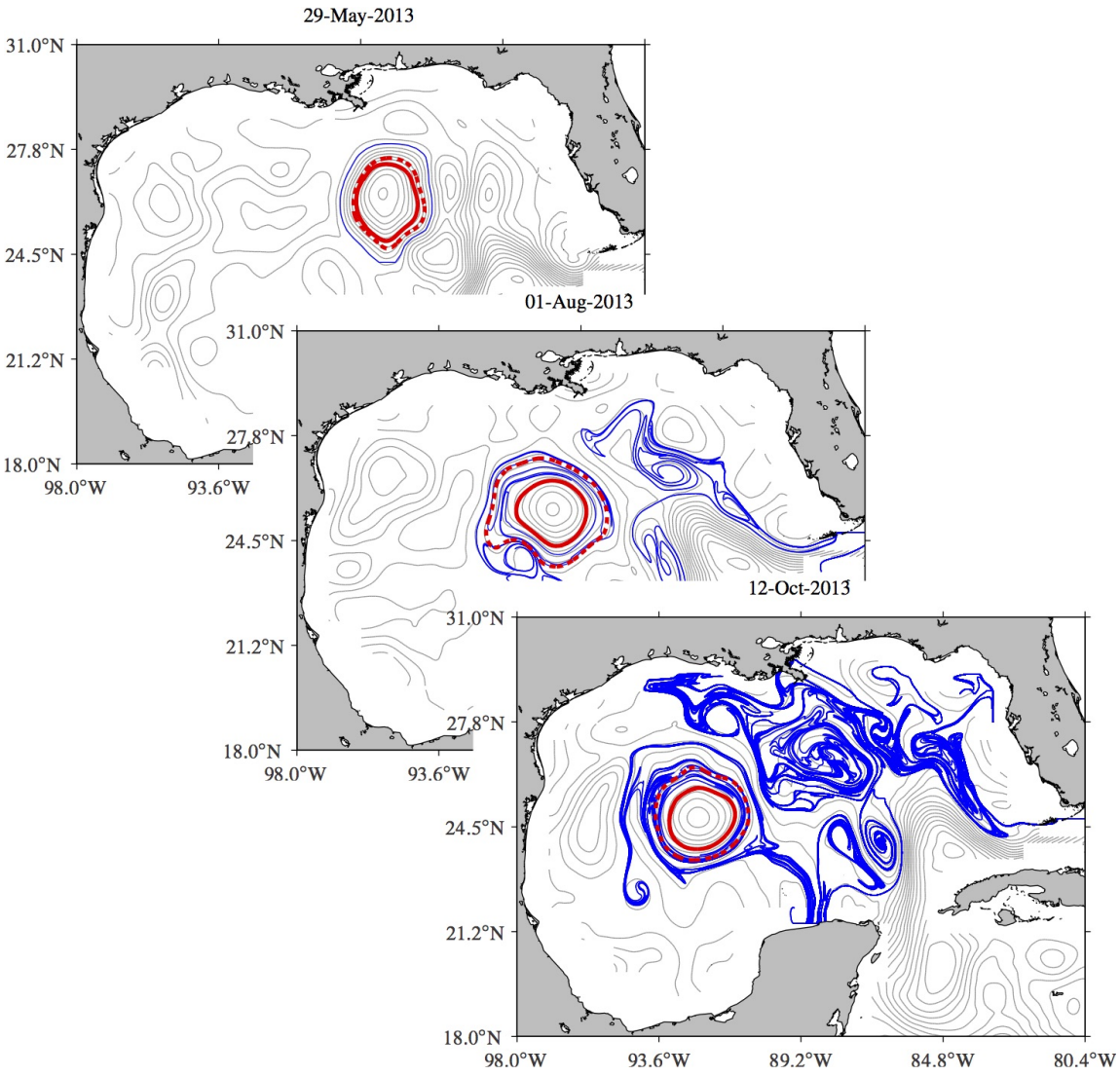

Figure 1: In grey, contour levels of the altimetric sea surface height (SSH) field in the Gulf of Mexico (GoM) on selected days. Overlaid in blue are snapshots of the passive evolution, according to the altimetry-derived flow, of tracers initially on 29 May 2013 along the outermost of the closed SHH streamlines filling a mesoscale region of nearly 100-km radius in the center of the GoM, which has been identified as a Loop Current ring (LCR) and named *Kraken*. These closed instantaneous SSH streamlines are the Eulerian footprints of a coherent Lagrangian LCR, which nearly steadily translates westward across the GoM. The solid red curve is the boundary for the longest-lived and largest coherent Lagrangian LCR core. The dashed red curve is a material loop that provides repeated, short-term shielding to this core.

Geodesic eddy detection has been designed to unveil the precise location of such long- and short-term resilient material loops. These are indicated by a solid and dashed red curve, respectively, in Fig. 1. To unveil them, we applied geodesic eddy detection on the altimetry-derived velocity field over the time interval $[t_0, t_0 + T]$ for appropriate choices of t_0 and T.

The specific choices $t_0 = 29$ May 2013 and $T = 200$ d were found to produce a resilient material loop that provides the boundary for the largest and longest-lived coherent Lagrangian ring core. From $t_0 = 29$ May 2013 to $t_0 + T = 15$ December 2013, this boundary uniformly stretches by a factor $\lambda = 1.05$. This minor uniform stretching of the boundary along with the conservation of the enclosed area, which holds because the velocity field is geostrophic and hence divergenceless, conveys LCR *Kraken* formidable Lagrangian coherence.

Shorter-term resilient material loops encompassing the largest area which includes the long-term coherent Lagrangian ring core are found from the application of geodesic eddy detection every t_0 from 29 May daily through 15 December 2013 using $T = 30$ d. These emerging material loops reassume their initial arclength (i.e., they have $\lambda = 1$) after a period of one month. As such, they convey additional temporary but repeated shielding to the ring core, reinforcing its coherent Lagrangian nature. Successive short-term coherence regain events where first reported by Wang *et al.* (2016) for Agulhas rings in the South Atlantic.

Beyond the fact that our inference on the formidable Lagrangian coherence of LCR *Kraken* remains valid irrespective of the reference frame adopted by the observer, a unique aspect of geodesic eddy detection, the pertinent question that arises is whether this is a real ingredient of the ocean circulation in the GoM or is just an artifact of the limitation of satellite altimetry to resolve submesoscale and likely ageostrophic motions. It turns out that, as we proceed to show, LCR *Kraken* constitutes to a large extent a coherent Lagrangian ring. We support our demonstration on two pieces of independent observations, rarely available

simultaneously over an extended period of time.

The first piece of observations is given by satellite ocean color. Figure 2 shows snapshots of chlorophyll concentration on selected days with the altimetry-inferred long- and short-term coherent Lagrangian ring boundaries overlaid (solid and dashed red, respectively). Weekly snapshots in the period 19 April through 21 November 2013 are shown in Supplementary Movie S2.

Note the patch of low chlorophyll concentration which, for a period as long as about seven months, quite closely accompanies the altimetry-inferred coherent Lagrangian ring as it nearly steadily translates westward in the GoM. Note also that the origin of the chlorophyll defect can be traced completely into the Caribbean Sea, which is characterized by predominantly oligotrophic conditions (Gómez, 2014). This indicates that the formation of LCR *Kraken* follows the standard scenario: the Loop Current occludes and LCR *Kraken* is subsequently pinched off from the current. This process is Lagrangian in essence (Andrade-Canto *et al.*, 2013). Altogether the two observations just made provide strong support to our conclusion that LCR *Kraken* is largely Lagrangian.

Clearly, some deviations between the boundaries of the low-chlorophyll patch and the altimetry-inferred coherent Lagrangian ring are evident. But these can be expected because of at least two reasons. First, cloud coverage is important at times during the observational period. This results in nonuniform sampling, which impacts the interpolation of the data on a regular grid and hence the resolution of the chlorophyll defect. Second, chlorophyll as a tracer cannot be considered to be entirely passive. Vertical pumping of nutrients at the periphery of LCR *Kraken* may be expected (Mahadevan *et al.*, 2008). Biological activity stimulated by nutrient availability may be modifying the chlorophyll concentration and thus the size of the patch as it translates across the GoM.

However, the geodesically detected long- and short-term Lagrangian boundaries much better constrain the extent of the chlorophyll deficient patch than instantaneous closed streamlines of the SSH field. This is demonstrated in the top-right panel of Fig. 2, which

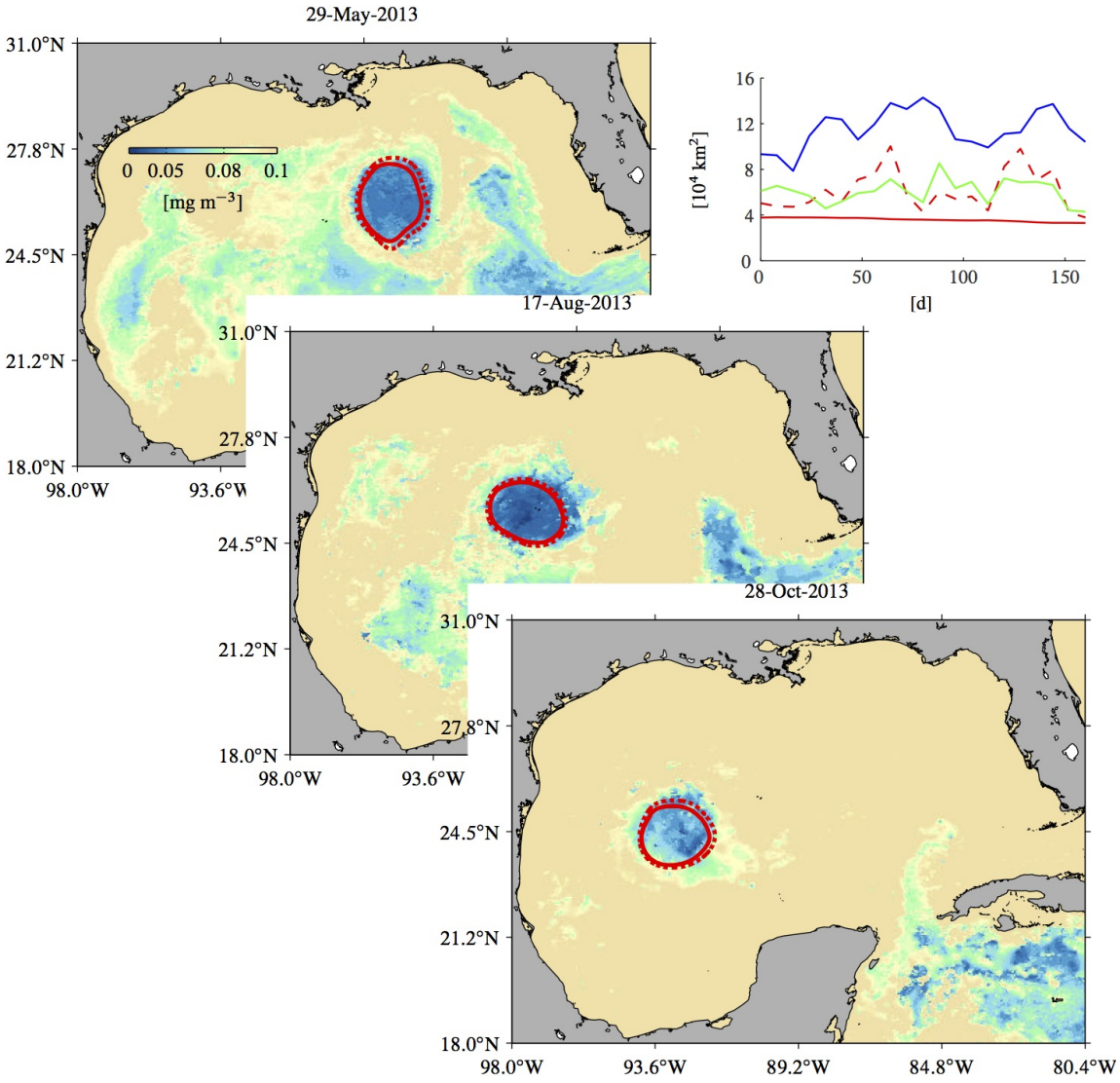

Figure 2: Satellite-derived chlorophyll concentration images on selected days with the altimetry-inferred long- (solid) and short-term (dashed) coherent Lagrangian boundaries of LCR *Kraken* overlaid. The top-right panel shows, as a function of time since 29 May 2013, area enclosed by the long- (solid red) and short-term (dashed red) Lagrangian boundaries, the outermost instantaneous closed SSH contour level (blue), and the area spanned by the chlorophyll deficient patch (green).

compares, as a function of time since 29 May 2013, the area enclosed by the long- (solid red) and short-term (dashed red) Lagrangian boundaries and the outermost instantaneous closed SSH contour level (blue) with the area spanned by the chlorophyll deficient patch (green), whose boundary was determined as the chlorophyll isoline where the concentration change with respect to the area enclosed by it is highest. Note that the area of the chlorophyll deficient patch is not constant as is (to numerical error) that enclosed by the long-term boundary. While biological activity is likely acting to shape the form and extent of the patch, this action is constrained by the Lagrangian circulation, which favors coherence regain events that prevent the chlorophyll depleted water from spreading away from LCR *Kraken*.

The second piece of observations is provided by trajectories of satellite-tracked surface drifters. As part of the routine monitoring of LCRs, the Horizon Marine Inc.'s EddyWatch® program deployed various drifters in the vicinity of LCR *Kraken* along its westward path. Figure 3 shows snapshots of the evolution of the altimetry-inferred coherent Lagrangian ring long- and short-term boundaries, indicated by solid and dashed red curves, respectively, along with that of drifters initially lying within these boundaries or which at some point in time have come as close as 50 km to the long-term boundary (various additional snapshots are shown in Supplementary Movie S3). One point on the long-term boundary is highlighted by a black dot surrounded by a circle, for reference. The drifter positions are indicated by blue dots on the specified day. The tails (in blue) attached to the dots are week-long past trajectory segments.

The first aspect to note is that the drifters deployed inside or near by the long- and short-term boundaries tend to remain in their vicinity, very closely following the anticyclonic circulatory motion of passive tracers along them. This can be most easily visualized by comparing the position of the point highlighted on the long-term boundary and those of the nearby drifters. The turnover timescale of that point is of about two weeks, which is nearly the same for the drifters in its vicinity. Overall the behavior of the drifters is largely

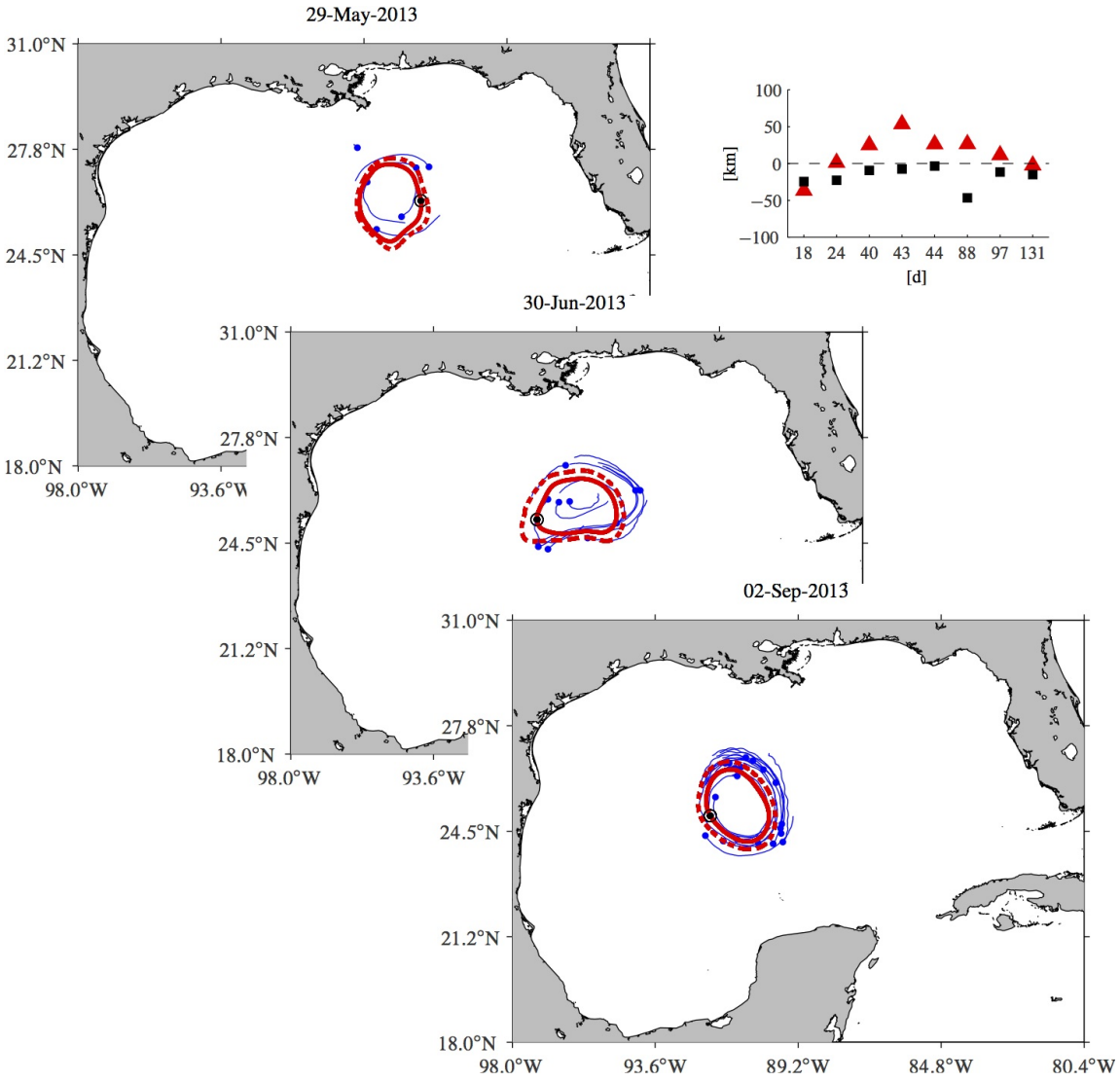

Figure 3: Snapshots of the evolution of the altimetry-inferred coherent Lagrangian long- (solid red) and short-term (dashed red) boundaries of LCR *Kraken* along with that of satellite-tracked surface drifters initially as close as 50 km from the long-term boundary (blue). The drifter positions on each day shown are indicated by blue dots. The tails attached to the dots are week-long past trajectory segments. One point on the long-term boundary is highlighted by a black dot surrounded by a circle, for reference. The top-right panel shows as a function of drifter lifespan, initial (black square) and mean (red triangle) shortest signed distance to the long-term boundary for all drifters initially lying within.

consistent with the motion of tracer particles passively advected by the altimetry-derived flow. This provides further support to the Lagrangian nature of LCR *Kraken* inferred from the analysis of altimetry data.

A quantitative assessment of the above qualitative observations is provided in the top-right panel of Fig. 3, which shows, as a function of drifter lifespan, initial (black square) and mean (red triangle) shortest signed distance to the long-term coherent Lagrangian boundary of LCR *Kraken* for all drifters initially lying within (a negative value indicates that the drifter is inside the boundary). Two out of 8 drifters spent their whole lifespan (18 and 131 d) within the long-term boundary. The other 6 drifters remained around the ring with a mean minimum distance shorter than 50 km.

Inertial effects (i.e., of objects' finite size and buoyancy) might explain the behavior of the relatively slow outward moving drifters. Indeed, floating objects are predicted to be repelled away from anticyclonic coherent Lagrangian eddies (Beron-Vera *et al.*, 2015; Haller *et al.*, 2016). These effects can be expected to be most effective when the para-drogues attached to the drifters are closed. The outward motion of the drifters may be indicative of this. Windage may also explain deviations of drifter motion from purely Lagrangian motion. However, while windage effects near mesoscale eddies or rings have not been well constrained for biological tracers (McGillicuddy *et al.*, 1998; McGillicuddy *et al.*, 2007; Mahadevan *et al.*, 2008), they may be outbalanced by inertial effects (Beron-Vera *et al.*, 2016; , Supplementary Information).

An additional important aspect to be highlighted of the behavior of the drifters is the relative absence of submesoscale wiggles in their hourly-sampled trajectories. The lack of such wiggles in the drifter trajectories is largely consistent with the convexity of the altimetry-inferred long- and short-term coherent Lagrangian ring boundaries. This observation gives further support to the significance of the altimetry-based inference.

It might be argued that the dominance of wiggle-free drifter trajectories is a consequence of the drifters being para-drogued at about 50-m depth. However, this should

not prevent the drifters from sampling submesoscale motions if they were active (Pérez-Brunius *et al.*, 2013; Lumpkin, 2015). Indeed, loops of about 10-km or smaller diameter can be seen at times mounted on the drifter trajectories. But the frequency of those loops is typically very close to the local Coriolis frequency, as it has been observed earlier in the same region using the same drifters (Anderson and Sharma, 2008). So the loops mainly correspond to near-inertial oscillations, which do not impact relative dispersion statistics (Beron-Vera and LaCasce, 2016) and thus should not be expected to constitute an effective mechanism for the erosion of mesoscale coherent Lagrangian structures such as the resilient material boundary around LCR *Kraken*.

It is still of interest to investigate if mesoscale coherent Lagrangian eddies can be realized in the presence of submesoscale motions. We carried such an investigation by seeking evidence of coherent Lagrangian LCR *Kraken* in the data-assimilative submesoscale permitting NCOM simulation of the GoM. The bottom-left panel of Fig. 4 shows a snapshot of the surface vorticity (ω) normalized by the mean Coriolis parameter in the GoM (f) from this simulation, which reveals a large number of eddy-like features spanning scales in the meso- and submesoscale ranges. Note in particular the suprainertial ($|\omega|/f > 1$) submesoscale eddies rolling around the mesoscale eddy feature in the center of the GoM, which appears to be the signature of LCR *Kraken* in the model vorticity field.

However, we have not been able to extract a mesoscale coherent Lagrangian ring akin to LCR *Kraken* from the NCOM upper ocean (surface, 10, and 50-m levels) velocity field on any day and for any coherence timescale choice or stretching parameter. But we have found that a velocity field computed geostrophically using subsampled model SSH sustains a Lagrangian ring with $T = 80$ d coherence horizon. The procedure employed to obtain the subsampled SSH field mimicked that used to construct an SSH field by interpolating along-track satellite altimetry measurements. Figure 4 shows snapshots of the evolution of the extracted coherent Lagrangian boundary (dark blue) along with the boundary obtained from satellite altimetry (red). While the boundaries do not coincide exactly or

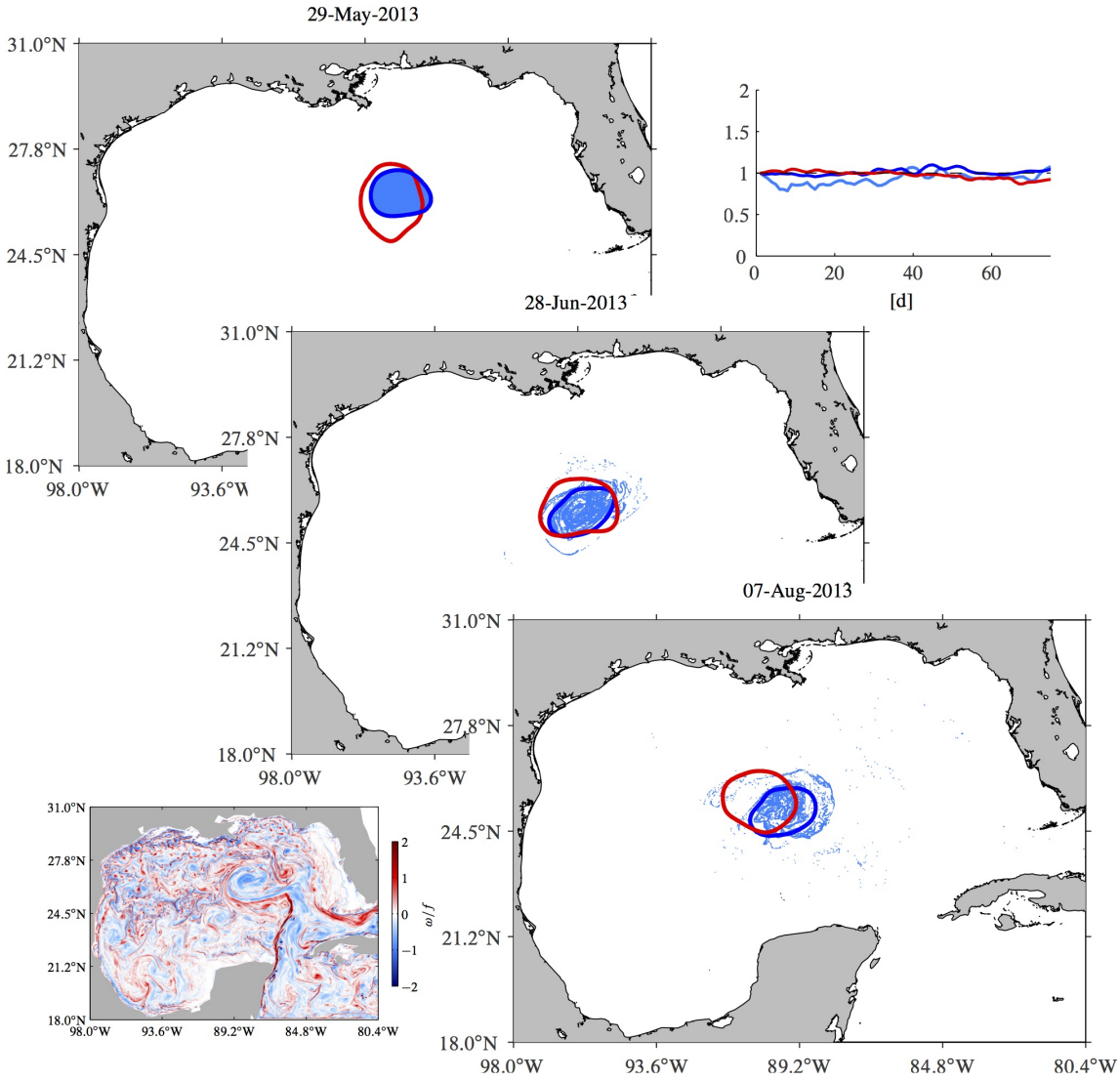

Figure 4: Snapshots of the evolution of the boundary of coherent Larangian LCR *Kraken* as extracted from altimetric SSH (red) and subsampled SSH from a submesoscale permitting Navy Coastal Model (NCOM) simulation of the GoM (blue), and a tracer patch passively advected by the surface model velocity (light blue). The top-right panel shows the mean distance to the corresponding centroid from points on the altimetry-derived boundary (red), the model SSH-derived boundary (blue), and the boundary of the tracer patch passively advected by the surface model velocity (light blue), each normalized by the value taken initially on 29 May 2013. The bottom-left panel is snapshot of the surface vorticity (normalized by the mean Coriolis parameter) field on 29 May 2013.

enclose the same area, they lie nearby. Additionally, the long-range transport ability of the coherent Lagrangian ring obtained from simulated altimetry is shorter than that of the ring extracted from satellite altimetry. These differences in Lagrangian behavior, which are not obvious from the comparison of model and satellite altimetry SSH fields, suggest a means for constructing model performance metrics.

But the pertinent question is whether the simulated total surface velocity field supports some form of mesoscale Lagrangian coherence. We investigated this by advecting under the total surface model velocity passive tracers initially within the coherent Lagrangian boundary detected from simulated altimetry. This numerical experiment revealed the existence of a swirling Lagrangian structure (light blue dots in Fig. 4) which, while experiencing filamentation, prevailed in large part confined within the interior of the boundary obtained from simulated altimetry. A compactness measure (Haralick, 1974) of this structure is provided in the top-right panel of Fig. 4, which shows the mean distance to the corresponding centroid from points on the altimetry-derived boundary (red), the boundary obtained from simulated altimetry (blue), and the boundary of the tracer patch passively advected by the surface model velocity (light blue), each normalized by the value taken initially on 29 May 2013. Note that the compactness measure remains close to one for the boundaries extracted from satellite and simulated altimetry consistent with their coherent Lagrangian nature. The departure from one can be larger for the tracer patch, but this is never in excess of 0.25.

These numerical results suggest that mesoscale Lagrangian coherence is indeed realizable in the presence of active submesoscale motions, albeit not in the mathematically well-constrained form as it commonly emerges from geostrophic velocity derived using coarse satellite altimetry data. Such an idealized form of mesoscale Lagrangian coherence is observable, however, as we have shown here using spatiotemporally and dynamically less restrained data from independent sources. But even when it is solely supported by the altimetry-derived geostrophic flow, some form of mesoscale Lagrangian coherence, which

awaits formal characterization, can be expected to be sustained by the actual flow.

4. Concluding remarks

In this paper we have provided independent observational support for the existence of a coherent Lagrangian eddy in the ocean. Such eddies have material boundaries that do not filament or experience global break away over long periods of time. A recent technique rooted in nonlinear dynamical systems theory, geodesic eddy detection, has been specifically designed to unveil these eddies from a velocity realization in an completely observer-independent fashion. We have focused on a Loop Current ring (LCR) in the Gulf of Mexico (GoM) which has been detected from its Eulerian footprints in satellite altimetry sea surface height (SSH) data and termed *Kraken*.

Applying geodesic eddy detection on the altimetry-derived velocity field, we inferred that LCR *Kraken* possessed a Lagrangian core of about 100-km radius, surrounded by a resilient boundary that remained so for a period as long as seven months. Lagrangian boundaries with similar but shorter-lived resiliency, which enclosed a larger domain including this core, were found to emerge over this period. These boundaries conveyed further Lagrangian coherence to LCR *Kraken*.

The observational support for the altimetry-inferred material coherence was obtained from two, rarely available simultaneously, independent sources: satellite ocean color and satellited-tracked surface drifter trajectories. A low-concentration chlorophyll patch traceable into the Caribbean Sea accompanied LCR *Kraken* in its nearly steady westward translation across the GoM. The surface drifters, in turn, developed relatively wiggle-free anticyclonic loops inside or immediately outside LCR *Kraken*'s Lagrangian core with turnover times (of two weeks or so) very close to those of passive tracer particles circling along the boundary of the core.

The output from a data-assimilative submesoscale permitting simulation of the GoM based on the Navy Coastal Ocean Model (NCOM) was finally analyzed in search for

traces of the coherent Lagrangian LCR detected from altimetry. While no coherent Lagrangian ring was possible to be detected from the model upper velocity, a swirling Lagrangian structure was revealed in the vicinity of a coherent Lagrangian ring sustained by the geostrophic flow derived from subsampled model SSH. This indicated that submesoscale motions, when active, need not necessarily always act to erode the signature of mesoscale coherent Lagrangian structures detected from geostrophic flow derived using coarse satellite altimetry data.

Subject of ongoing investigation is the isolation and formal classification of the possible forms of Lagrangian coherence, at both meso- and submesoscales, sustained by velocity fields produced by high-resolution model simulations.

Acknowledgments. The altimeter products were produced by SSALTO/DUCAS and distributed by AVISO with support from CNES (http:// www.aviso.oceanobs). The ocean color products were produced and distributed by NASA OBPG. The surface drifters were deployed as part of Horizon Marine Inc.'s EddyWatch® program. The data have been provided as a part of a data exchange agreement between Horizon Marine Inc. and PEMEX under CICESE–PEMEX SAP contracts 428217896, 428218855, and 428229851. The quality control and post-processing of these data were carried out by Paula García and Argelia Ronquillo. The NCOM simulation was produced at the Naval Research Laboratory and can be obtained from http:// dx.doi.org/10.7266/N7FQ9TJ6, N76Q1V5G, and N72Z13F4. Support for this work was provided by the Gulf of Mexico Research Initiative (MJO, FJBV, and YW) as part of the Consortium for Advanced Research on Transport of Hydrocarbon in the Environment (CARTHE); SENER–CONACyT grant 201441 (MJO, FJBV, PPB) as part of the Consorcio de Investigación del Golfo de México (CIGoM); and NOAA/AOML and UM/CIMAS (JT).

REFERENCES

Anderson, S. P. and N. Sharma. 2008. Satellite-tracked drifter measurements of inertial currents in the Gulf of Mexico. In *Proceedings of the IEEE/OES/CMTC Ninth Working Conference on Current Measurement Technology.*, pages 285–288. IEEE Computer Society.

Andrade-Canto, F., J. Sheinbaum, and L. Z. Sansón. 2013. A Lagrangian approach to the Loop Current eddy separation. Nonlin. Processes Geophys., *20*, 85–96.

Barron, C. N., A. B. Kara, P. J. Martin, R. C. Rhodes, and L. F. Smedstad. 2006. Formulation, implementation and examination of vertical coordinate choices in the global Navy Coastal Ocean Model (NCOM). Ocean Modell., *11*, 347–375.

Barron, C. N., L. F. Smedstad, J. M. Dastugue, and O. M. Smedstad. 2007. Evaluation of ocean models using observed and simulated drifter trajectories: Impact of sea surface height on synthetic profiles for data assimilation. J. Geophys. Res., *112*, C07019. doi: 0.1029/2006JC002982.

Beron-Vera, F. J., M. J. Olascoaga, and G. J. Goni. 2008. Oceanic mesoscale vortices as revealed by Lagrangian coherent structures. Geophys. Res. Lett., *35*, L12603. doi: 10.1029/2008GL033957.

Beron-Vera, F. J., M. J. Olascoaga, and G. J. Goni. 2010. Surface ocean mixing inferred from different multisatellite altimetry measurements. J. Phys. Oceanogr., *40*, 2466–2480. doi: 10.1175/2010JPO4458.1.

Beron-Vera, F. J., Y. Wang, M. J. Olascoaga, G. J. Goni, and G. Haller. 2013. Objective detection of oceanic eddies and the Agulhas leakage. J. Phys. Oceanogr., *43*, 1426–1438.

Beron-Vera, F. J., M. J. Olascoaga, G. Haller, M. Farazmand, J. Triñanes, and Y. Wang. 2015. Dissipative inertial transport patterns near coherent Lagrangian eddies in the ocean. Chaos, *25*, 087412. doi: 10.1063/1.4928693.

Beron-Vera, F. J., M. J. Olascoaga, and R. Lumpkin. 2016. Inertia-induced accumulation of flotsam in the subtropical gyres. Geophys. Res. Lett, *43*, 12228–12233. URL https://arxiv.org/abs/1606.02649.

Beron-Vera, F. J. and J. H. LaCasce. 2016. Statistics of simulated and observed pair separations in the gulf of mexico. J. Phys. Oceanorg, *46*(7), 2183–2199. doi: 10.1175/JPO-D-15-0127.1.

Cummings, J. A. 2005. Operational multivariate ocean data assimilation. Q. J. Royal Meteorol. Soc., *131*, 3583–3604.

Fu, L. L., D. B. Chelton, P.-Y. Le Traon, and R. Morrow. 2010. Eddy dynamics from satellite altimetry. Oceanography, *23*, 14–25.

Gómez, R. A. 2014. Spectral reflectance analysis of the Caribbean Sea. Geof. Int., *53-4*, 385–398.

Hadjighasem, A. and G. Haller. 2016. Geodesic transport barriers in Jupiter's atmosphere: a video-based analysis. SIAM Review, *58*, 69–89.

Hadjighasem, A., M. Farazmand, and G. Haller. 2013. Detecting invariant manifolds, attractors, and generalized KAM tori in aperiodically forced mechanical systems. Nonlinear Dyn., *73*, 689–704.

Haller, G. 2015. Lagrangian coherent structures. Ann. Rev. Fluid Mech., *47*, 137–162. doi: 10.1146/annurev-fluid-010313-141322.

Haller, G. 2016. Climate, black holes and vorticity: How on Earth are they related? SIAM News, *49*, 1–2.

Haller, G. and F. J. Beron-Vera. 2012. Geodesic theory of transport barriers in two-dimensional flows. Physica D, *241*, 1680–1702. doi: 10.1016/j.physd.2012.06.012.

Haller, G. and F. J. Beron-Vera. 2013. Coherent Lagrangian vortices: The black holes of turbulence. J. Fluid Mech., *731*, R4. doi: 10.1017/jfm.2013.391.

Haller, G. and F. J. Beron-Vera. 2014. Addendum to 'Coherent Lagrangian vortices: The black holes of turbulence'. J. Fluid Mech., *755*, R3.

Haller, G., A. Hadjighasem, M. Farazmand, and F. Huhn. 2016. Defining coherent vortices objectively from the vorticity. J. Fluid Mech., *795*, 136–173.

Haralick, R. M. 1974. A measure for circularity of digital figures. IEEE Transactions on Systems, Man and Cybernetics, *4*, 334–336.

Haza, A., T. M. Özgökmen, and P. J. Hogan. 2016. Impact of submesoscales on surface material distribution in a gulf of mexico mesoscale eddy. Ocean Modelling, *107*, 28–47.

Karrasch, D., F. Huhn, and G. Haller. 2014. Automated detection of coherent Lagrangian vortices in two-dimensional unsteady flows. Proc. Royal Soc. A, *471*, 20140639.

Klein, P. 2009. The oceanic vertical pump induced by mesoscale and submesoscale turbulence. Ann. Rev. Marine Sci., *1*, 351–375.

Le Traon, P. Y., F. Nadal, and N. Ducet. 1998. An improved mapping method of multi-satellite altimeter data. J. Atmos. Oceanic Technol., *15*, 522–534.

Leben, R. R. 2005. Altimeter-derived loop current metrics. In Sturges, W. and A. Lugo-Fernandez, editors, *Circulation in the Gulf of Mexico: Observations and Models*, pages 181–201. American Geophysical Union. ISBN 9781118666166. doi: 10.1029/161GM15.

Lumpkin, R. 2015. Global characteristics of coherent vortices from surface drifter trajectories. J. Geophys. Res., *121*, 1306–1321.

Lumpkin, R. and M. Pazos. 2007. Measuring surface currents sith Surface Velocity Program driftres: the instrument, its data and some recent results. In Griffa, A., A. D.

Kirwan, A. Mariano, T. Özgökmen, and T. Rossby, editors, *Lagrangian Analysis and Prediction of Coastal and Ocean Dynamics*, chapter 2, pages 39–67. Cambridge University Press.

Mahadevan, A., L. N. Thomas, and A. Tandon. 2008. Comment on "Eddy/wind interactions stimulate extraordinary mid-ocean plankton blooms". Science, *320*, 448b. doi: 10.1126/science.1152111.

McGillicuddy, D. J., A. R. Robinson, D. A. Siegal, H. W. Jannasch, R. Johnson, T. D. Dicky, J. Mcneil, A. F. Michaels, and A. H. Knap. 1998. Influence of mesoscale eddies on new production in the Sargasso Sea. Nature, *394*, 263–266.

McGillicuddy, D. J., L. A. Anderson, N. R. Bates, T. Bibby, K. O. Buesseler, C. A. Carlson, C. S. Davis, C. Ewart, P. G. Falkowski, S. A. Goldthwait, D. A. Hansell, W. J. Jenkins, R. Johnson, V. K. Kosnyrev, J. R. Ledwell, Q. P. Li, D. A. Siegel, and D. K. Steinberg. 2007. Eddy/wind interactions stimulate extraordinary mid-ocean plankton blooms. Science, *316*(5827), 1021–1026. doi: 10.1126/science.1136256.

McWilliams, J. C. 2008. Fluid dynamics at the margin of rotational control. Environ. Fluid Mech., *8*, 441–449.

Metzger, E. J., O. M. Smedstad, and S. N. Carroll. 2009. User's Manual for Global Ocean Forecast System (GOFS) Version 3.0 (V3.0). NRL Memorandum Report, NRL/MR/7320-09-9175.

NRL. 1997. The Naval Research Laboratory's Coupled Ocean/Atmosphere Mesoscale Prediction System (COAMPS). Mon. Weather Rev. 125, 1414-1430.

Olascoaga, M. J., F. J. Beron-Vera, G. Haller, J. Trinanes, M. Iskandarani, E. F. Coelho, B. Haus, G. J. H. S. Huntley, A. D.Kirwan, Jr., B. L. Lipphardt, Jr., T. Özgökmen, A. J. H. M. Reniers, and A. Valle-Levinson. 2013. Drifter motion in the Gulf of Mexico

constrained by altimetric Lagrangian Coherent Structures. Geophys. Res. Lett., *40*, 6171–6175. doi: 10.1002/2013GL058624.

Onu, K., F. Huhn, and G. Haller. 2015. LCS Tool: A computational platform for Lagrangian coherent structures. J. Comp. Sci., *7*, 26–36.

Pérez-Brunius, P., P. García-Carrillo, J. Dubranna, J. Sheinbaum, and J. Candela. 2013. Direct observations of the upper layer circulation in the southern Gulf of Mexico. Deep Sea Res. II, *85*, 182–194. ISSN 0967-0645. doi: http://dx.doi.org/10.1016/j.dsr2.2012.07.020.

Poje, A. C., T. M. Özgökmen, B. Lipphart, Jr., B. Haus, E. Ryan, A. C. Haza, G. Jacobs, M. J. O. A. Reniers, G. Novelli, A. Griffa, F. J. Beron-Vera, S. Chen, P. Hogan, E. Coelho, A. Kirwan, Jr., H. Huntley, and A. Mariano. 2014. The nature of surface dispersion near the Deepwater Horizon oil spill. Proc. Nat. Acad. Sci. USA, *111*, 12693–12698.

Poulain, P.-M., R. Gerin, E. Mauri, and R. Pennel. 2009. Wind effects on drogued and undrogued drifters in the eastern Mediterranean. J. Atmos. Oceanic Technol., *26*, 1144–1156.

Rio, M.-H. and F. Hernandez. 2004. A mean dynamic topography computed over the world ocean from altimetry, in situ measurements, and a geoid model. J. Geophys. Res., *109*, C12032. doi: 10.1029/2003JC002226.

Romero, I. C., T. Özgökmen, S. Snyder, P. Schwing, B. J. O'Malley, F. J. Beron-Vera, M. J. Olascoaga, P. Zhu, E. Ryan, S. S. Chen, D. L. Wetzel, D. Hollander, and S. A. Murawski. 2016. Tracking the Hercules 265 marine gas well blowout in the Gulf of Mexico. J. Geophys. Res., *121*(1), 706–724. doi: 10.1002/2015JC011037.

Rowley, C. and A. Mask. 2014. Regional and coastal prediction with the relocatable ocean nowcast/forecast system. Oceanography, *27*, 3. doi: 10.5670/oceanog.2014.67.

Sharma, N., P. Brickley, G. Owen, and P. Coholan. 2010. Use of air-deployed drogued drifting buoys for oil spill tracking. In *OCEANS 2010*, pages 1–9. IEEE Computer Society.

Smith, S. R., J. A. Cummings, P. Spence, S. N. Carroll, C. Rowley, O. M. Smedstad, P. Chu, B. Lunde, J. Shriver, and R. Helber. 2011. Validation Test Report for the Navy Coupled Ocean Data Assimilation 3D Variational Analysis (NCODA-VAR) System, Version 3.43. NRL Memorandum Report NRL/MR/7320-11-9363.

Wang, Y., M. J. Olascoaga, and F. J. Beron-Vera. 2015. Coherent water transport across the South Atlantic. Geophys. Res. Lett., *42*, 4072–4079. doi: 10.1002/2015GL064089.

Wang, Y., M. J. Olascoaga, and F. J. Beron-Vera. 2016. The life cycle of a coherent Lagrangian Agulhas ring. J. Geophys. Res., *121*, 3944–3954. doi: 10.1002/2015JC011620.